Pramana – J. Phys. (2020) 94:107
https://doi.org/10.1007/s12043-020-01966-1

Ab-initio study of ordered III–V antimony-based semiconductor alloys $GaP_{1-x}Sb_x$ and $AlP_{1-x}Sb_x$

F ANNANE[1,2], H MERADJI[2,*], S GHEMID[2], H BENDJEDDOU[2], F EL HAJ HASSAN[3], VIPUL SRIVASTAVA[4] and R KHENATA[5]

[1]Département de Physique, Université 20 Août 1955, Skikda, Algeria
[2]Laboratoire LPR, Département de Physique, Faculté des Sciences, Université Badji Mokhtar, Annaba, Algeria
[3]Laboratoire de Physique et d'Electronique, Faculté des Sciences I, Université Libanaise, El-Hadath, Beirut, Lebanon
[4]Department of Physics, School of Chemical Engineering and Physical Sciences, Lovely Professional University, Phagwara 144 411, India
[5]Laboratoire de Physique Quantique de la Matière et de la Modélisation Mathématique (LPQ3M), Université de Mascara, 29000 Mascara, Algeria
*Corresponding author. E-mail: hmeradji@yahoo.fr

MS received 1 November 2019; revised 29 February 2020; accepted 10 April 2020; published online 16 July 2020

Abstract. In this work, we have investigated the structural, electronic and thermodynamic properties of $GaP_{1-x}Sb_x$ and $AlP_{1-x}Sb_x$ ternary alloys for a number of ordered structures and compositions in a series of first-principles calculations within the density functional theory, using full potential-linearised augmented plane-wave (FP-LAPW) method, as implemented in the WIEN2k code. The exchange-correlation effect was treated within the generalised gradient approximation (GGA) in the form of GGA-PBEsol to optimise the structure and to compute the ground-state properties. In addition to the GGA, the modified Becke–Johnson (mBJ) potential coupled with the spin-orbit interaction (SOI) was also applied to obtain reliable results for the electronic properties. Our investigation on the effect of composition on lattice constant, bulk modulus and band gap showed almost nonlinear dependence on the composition. The $GaP_{1-x}Sb_x$ and $AlP_{1-x}Sb_x$ alloys are found to be semiconductors with a positive energy gap for the whole concentration range. The spin-orbit splitting Δ_{SO} was found to increase with Sb composition with a marginal bowing parameter. Besides, a regular-solution model was used to investigate the thermodynamic stability of the alloys which mainly indicates a phase miscibility gap. In addition, the quasiharmonic Debye model was applied to analyse the effect of temperature and pressure on the Debye temperature and heat capacity.

Keywords. Ternary III–V antimonides; full potential-linearised augmented plane-wave; spin-orbit interaction; band structure; miscibility gap; critical temperature.

PACS Nos **61.66.Dk; 71.15.Ap; 71.15.Mb; 71.20.−b; 65.40.−b**

1. Introduction

The use of III–V antimony-based semiconductors in devices has been extensively explored because they exhibit the smallest band gaps and highest mobilities among the III–V materials. Thus, these materials have the ability to span the range of wavelengths from the traditional wavelengths of interest for optical communication (1.3–1.5 μm) to much longer wavelengths (>15 μm) [1–6]. These antimony-based materials may offer the limit in III–V device performance in terms of speed, long wavelength for optoelectronics and quantum effects related to low effective mass. These materials have been used in both emitters and detectors that have spanned this extensive wavelength range. Some of these devices have utilised band-gap engineering to develop unique detectors and emitters using band offsets and strain. These devices range from simple detectors and LEDs to lasers with complex cascaded structure [7]. Their uses in electronic devices have been explored to a lesser extent, but unique devices are being developed that utilise the very high mobilities available in these small band-gap materials. The limited exploration of electronic devices is most likely due to the lack of a lattice-matched, semi-insulating substrate as well as the immaturity of the materials and growth science of

these materials compared to the more extensively examined arsenides, phosphides and nitrides. In the present work, we focus our attention on the two phosphide antimonides $GaP_{1-x}Sb_x$ and $AlP_{1-x}Sb_x$ alloys.

The ternary phosphide alloy $GaP_{1-x}Sb_x$ is potentially useful for opto-electronic device applications, and is a useful material for long-wavelength surface emitting lasers [8,9]. The adjustable band gap of $GaP_{1-x}Sb_x$ with composition [10] makes it a potentially useful material in fibre optic communication systems. The expected resonance enhancement of the hole-impact ionisation rate makes $GaP_{1-x}Sb_x$ a useful material for low-noise avalanche photodiodes using hole injection [11].

Although some experimental [12,13] and theoretical [14–17] investigations have been reported on the band-structure parameters of $GaP_{1-x}Sb_x$, many fundamental properties of this alloy remain to be determined precisely [18,19]. The successful growth of $AlP_{0.40}Sb_{0.60}$ lattice matched to InP has been reported [8]. This has encouraged people to investigate the properties of $AlP_{1-x}Sb_x$ ternary semiconductor alloys [20,21]. $AlP_{1-x}Sb_x$ is a very attractive material for optoelectronic applications. Several groups [22,23] have demonstrated that an AlPSb/GaPSb system has a large refractive index difference, which is useful for distributed Bragg reflectors (DBR) in InP-based vertical cavity surface emitting lasers (VCSELs) operating in the long-wavelength region, recognized as key devices for optical interconnection systems. Recently, both $GaP_{1-x}Sb_x$ and $AlP_{1-x}Sb_x$ alloys were selected as useful materials for the quantum dot intermediate band solar cell (QDSC) [24]. However, the large lattice mismatch between the GaP and GaSb lattice parameters, which are of the order of 11.15% and 11.65% between AlP and AlSb lattice parameters [25], as well as the existence of a miscibility gap ranging from $x = 0.01$ to 0.99, covering essentially the entire range of solid composition for GaPSb [13] and a complete miscibility gap predicted for AlPSb [26] causes difficulties in the growth of these alloys. The fundamental properties of the antimonides such as the low melting points and the lack of a stable antimony hydride introduce difficulties during the growth of such alloys. The growth of AlSb containing alloys has proven to be the most challenging of all the antimony containing III–V semiconductors. This difficulty is primarily due to the lack of suitable sources for the growth of AlSb at low temperatures and the resulting incorporation of excess amounts of carbon. As for the other Al-containing III–V semiconductors, oxygen incorporation was also found to be a problem which causes a chemically unstable species, and in some cases the heterogeneity and the contamination of the prepared materials make their application impossible.

All these difficulties explain the limited or lack or data for the fundamental properties for these ternary alloys over the entire range of composition and the absence of any experimental data in the literature about $AlP_{1-x}Sb_x$ alloys.

The band-gap energy is known to be one of the most important device parameters because it is strongly connected with the operating wavelength of the opto-electronic devices. Thus, the ability to calculate the electronic band structure and its derived properties of semiconductor alloys are important prerequisites for any analysis of the phenomena occurring in these alloys as well as in the related devices.

In the present contribution, the aim is to extend the study of the composition dependence of the energy band gap and to investigate in detail its derived properties. We have employed density functional theory (DFT); our calculations were all-electron ones, included the effect of spin-orbit interaction, which turns out to be especially important in the present system. Band structures are 'correct' due to the use of adequate exchange-correlation functional. In addition to the consideration of the electronic and the structural properties, we have studied the phase stability. In the subsequent text, the computational details are given in §2, the results are presented and discussed in §3 and the paper is concluded in §4.

2. Computational details

The calculations were performed in the framework of DFT [27] using specifically the full potential-linearised augmented plane-wave plus local orbital (FP-LAPW+lo) method [28,29] as implemented in WIEN2k code [30]. The exchange-correlation potential was treated within the GGA in the form of PBEsol proposed by Perdew *et al* [31] which is an improved form of the most popular Perdew–Burke–Ernzerhof (PBE) GGA [32]. This option was used to calculate ground-state properties and to optimise the structure parameters. In addition, insofar as the electronic properties are of interest, we recalculated them, applying the modified Becke–Johnson (mBJ) scheme [33] for the exchange-correlation potential. The mBJ potential is known to provide reasonably accurate band gaps of semiconductors and insulators with an orbital-independent exchange-correlation potential which depends solely on semilocal quantities. In the FP-LAPW+lo method, the wave function, charge density and potential were expanded by spherical harmonic functions inside non-overlapping spheres surrounding the atomic sites (muffin-tin spheres) and by plane-waves

basis set in the remaining space of the unit cell (interstitial region). To specify the parameters entering the calculation by the WIEN2k code, the maximal l value for the wave function expansion inside the atomic spheres was confined to $l_{\max}$ =10. The plane-wave cut-off of $K_{\max} = 8.0/R_{\mathrm{MT}}$ (R_{MT} is the smallest muffin-tin radius in the unit cell) was chosen for the expansion of the wave functions in the interstitial region while the charge density was Fourier expanded up to $G_{\max} = 14$ (Ryd)$^{1/2}$. The R_{MT} values were chosen for Al and P as 2.0 and for Ga and Sb as 2.1 and 2.2 au, respectively, in all calculations. The standard special k-points technique of Monkhorst and Park (MP) [34] was used for accurate Brillouin zone integrations. The k-mesh size was 12×12×12 MP special points for the binary compounds and 6×6×6 MP special points for the alloys. Accurate convergence criteria have been followed for all the above-mentioned parameters before handling the main study. The spin-orbit interaction (SOI) was added using second variational method with the scalar relativistic orbitals as the basis.

3. Results and discussion

3.1 *Structural properties*

In this section, the structural properties of the binary compounds GaP, GaSb, AlP and AlSb are analysed in the zinc blende structure. The alloys were modelled at some selected compositions $x = 0.25, 0.5, 0.75$ with ordered structures described in terms of periodically repeated supercells with eight atoms per unit cell. For the considered structures, we performed the structural optimisation by minimising the total energy with respect to the cell parameters and also the atomic positions. For the considered structures, the calculated total energy at many different volumes around equilibrium was fitted to the Murnaghan's equation of state [35] to obtain the equilibrium structural parameters of the binary compounds GaP, GaSb, AlP and AlSb and their ternary alloys $GaP_{1-x}Sb_x$ and $AlP_{1-x}Sb_x$ within the GGA-PBEsol approximation.

On the other hand, SOI becomes more significant for compounds containing heavy elements such as Sb because the potential near their nuclei is very strong and consequently the kinetic energy is very large, the electron velocity becomes comparable to the speed of light, leading to large relativistic corrections [36–38]. Therefore, the SOI has been considered and the results are compared with those of non-SOI calculation. For GaP, $GaP_{0.5}Sb_{0.5}$, GaSb and AlP, $AlP_{0.75}Sb_{0.25}$, AlSb, the SOI(non-SOI) equilibrium lattice constant are 5.445(5.444) Å, 5.818(5.818) Å, 6.111(6.108) Å and 5.473(5.473) Å, 5.671(5.670) Å, 6.157(6.158) Å, respectively. It should be noted that the SOI has a minor effect on obtaining the equilibrium lattice constants. Therefore, SOI was not included in the course of ground-state structure optimisations (done semi-relativistically).

The obtained results of the equilibrium lattice parameters, bulk modulus and its first pressure derivative are listed in tables 1 and 2 and are compared with the other experimental and theoretical predictions.

Our PBEsol results of lattice constant for the binary compounds agree well with the experimental data and similar to the recent ones calculated by FP-LAPW method within WC-GGA for GaP and GaSb compounds [17]. The results obtained for $GaP_{1-x}Sb_x$ alloys are in excellent agreement with the previous theoretical calculations of Chen and Ravindra [14] using projector augmented wave method.

Figure 1 shows the variation of the calculated equilibrium lattice constant with the concentration for $GaP_{1-x}Sb_x$ and $AlP_{1-x}Sb_x$ alloys. A large deviation from Vegard's law [65] is found with an upward bowing parameter equal to 0.168 Å for $GaP_{1-x}Sb_x$ and 0.142 Å for $AlP_{1-x}Sb_x$ alloys, obtained by fitting the calculated values with a polynomial function. The physical origin of this deviation should be mainly due to the large mismatches of the lattice constants of the binary compounds which are of the order of 11.15% and 11.65% between GaP–GaSb and AlP–AlSb lattice, respectively.

Unfortunately, there are no experimental and theoretical results for $AlP_{1-x}Sb_x$ ternary alloys to check the validity of this calculation. Therefore, the obtained results can be used to cover the lack of data in the literature for these ternary alloys.

Figure 2 shows the investigated bulk modulus (B) of $GaP_{1-x}Sb_x$ and $AlP_{1-x}Sb_x$ as a function of x. We observe that the estimated bulk modulus decreases when x increases. We can also remark that the bulk modulus makes a wide deviation from the linear concentration dependence (LCD), with opposite behaviour between the results of the lattice constants shown in figure 1. Most of the semiconductor materials and alloys of III–V group [66,67] follow this trend.

3.2 *Electronic properties*

The crucial role of the two studied ternary alloys in a variety of technological devices necessitates precise knowledge of the electronic properties such as the band structure and density of states (DOS). As was mentioned in §2, the band structure calculation has been done using mBJ exchange-correlation potential, to provide band-gap values which usually turn out to be in good agreement with the experimental data and this

Table 1. Calculated lattice constant (a), bulk modulus (B), first-order pressure derivative of bulk modulus (B'), band-gap (E_g) and split-off energy (Δ_{SO}) of $GaP_{1-x}Sb_x$ alloys compared with experimental and other theoretical results. Values calculated with and without taking SOI into account are listed.

Compounds	a (Å)	B (GPa)	B'	E_g (eV)	Δ_{SO} (meV)
GaP					
This work	5.444 PBEsol	85.071 PBEsol	4.575 PBEsol	2.306 mBJ 2.28 mBJ +SO	72.69 mBJ +SO
Experimental	5.45 [39]	88 [39]		2.260 [48] 2.35 [49]	80 [50]
Theoretical works	5.445 [17] 5.41 [40] 5.398 [41] 5.560 [42] 5.322 [43]	85.101 [17] 91.5 [40] 91 [41] 95 [42] 92 [43]	 4.5 [40] 4.76 [41] 4.34 [42]	1.68 [40] 1.59 [41] 2.32 [41] 2.263 [15] 2.289 [17]	82 [40] 86 [51]
$GaP_{0.75}Sb_{0.25}$					
This work	5.642 PBEsol	73.681 PBEsol	4.323 PBEsol	1.879 mBJ 1.787 mBJ +SO	229 mBJ +SO
Theoretical works	5.561 [14]			1.06 [14]	
$GaP_{0.5}Sb_{0.5}$					
This work	5.818 PBEsol	63.856 PBEsol	4.546 PBEsol	1.276 mBJ 1.146 mBJ +SO	404 mBJ +SO
Theoretical works	5.725 [14]			0.80 [14]	
$GaP_{0.25}Sb_{0.75}$					
This work	5.973 PBEsol	56.631 PBEsol	4.903 PBEsol	0.783 mBJ 0.631 mBJ +SO	495 mBJ +SO
Theoretical works	5.889 [14]			0.68 [14]	
GaSb					
This work	6.108 PBEsol	51.696 PBEsol	5.284 PBEsol	0.955 mBJ 0.753 mBJ +SO	655.69 mBJ +SO
Experimental	6.096 [44] 6.081 [45]	56.3 [44] 56 [45]		0.726 [44] 0.81 [49]	730 [52] 752 [53]
Theoretical works	6.107 [17] 6.214 [45] 6.115 [46] 5.981 [47]	51.895 [17] 44.627 [45] 51.9 [46] 56.7 [47]	4.822 [45] 5.0813 [45] 4.662 [47]	0.396 [46] 0.719 [15]	670 [40] 714 [51]

agreement is of the same order which can be achieved with computationally expensive GW (convolution of Green's function G and this screened Coulomb interaction W) or hybrid functional methods [68]. The SOI has also been considered for electronic calculation and the results are compared with those of non-SOI calculation. For electronic calculations, it is important to take SOI effects into account because the hole effective masses are strongly dependent on this interaction even when the heavier materials in this group such as GaSb and AlSb are considered. Results for the electronic band structures obtained with non-SOI and SOI are displayed in figures 3 and 4 for selected materials. The Fermi level (E_F) is set to zero energy. An indirect band gap has been observed for AlP, GaP and AlSb compounds, where the valence band maximum (VBM) and conduction band minimum (CBM) occur at Γ and X points, respectively, and a direct gap at Γ for GaSb. The results are presented in tables 1 and 2. It can be seen from figures 3 and 4 that SOI has a minor effect on the profile of the band structure, no bands cross E_F and a positive band gap appears for all selected structures which indicate a semiconductor gap behaviour for all the values of concentration. The figures also show that the conduction band moves towards the Fermi level by incorporating SOI in the potential with increasing Sb composition.

The calculated band-gap energies of the considered alloys using both non-SOI and SOI within mBJ scheme are presented in tables 1 and 2. The values obtained for the band gap with SOI are smaller than the non-SOI ones and are in better agreement with the available experimental results. It is clear that the degenerate states at high symmetry points split after the inclusion of SOI.

Table 2. Calculated lattice constant (a), bulk modulus (B), first-order pressure derivative of bulk modulus (B'), band-gap (E_g) and split-off energy (Δ_{SO}) of $AlP_{1-x}Sb_x$ alloys compared with experimental and other theoretical results. Values calculated with and without taking SOI into account are listed.

Compounds	a (Å)	B (GPa)	B'	E_g (eV)	Δ_{SO} (meV)
AlP					
This work	5.473 PBEsol	86.515 PBEsol	4.050 PBEsol	2.314 mBJ 2.295 mBJ +SO	53.73 mBJ +SO
Exp.	5.47 [39]	86 [39]		2.5 [59] 2.52 [18]	70 [61]
Other works	5.507 [54] 5.44 [40] 5.436 [41] 5.511 [41]	82.619 [54] 89 [40] 89 [41] 82 [41]	4.054 [54] 4.20 [40] 4.14 [41] 3.99 [41]	1.54 [40] 2.570 [54]	59 [51] 60 [40]
$AlP_{0.75}Sb_{0.25}$					
This work	5.671 PBEsol	74.368 PBEsol	4.097 PBEsol	2.011 mBJ 1.945 mBJ +SO	213.00 mBJ +SO
$AlP_{0.5}Sb_{0.5}$					
This work	5.851 PBEsol	65.360 PBEsol	4.189 PBEsol	1.716 mBJ 1.607 mBJ +SO	369.00 mBJ +SO
$AlP_{0.25}Sb_{0.75}$					
This work	6.013 PBEsol	58.397 PBEsol	4.236 PBEsol	1.569 mBJ 1.435 mBJ +SO	472 mBJ +SO
AlSb					
This work	6.158 PBEsol	53.210 PBEsol	4.447 PBEsol	1.796 mBJ 1.620 mBJ +SO	620.39 mBJ +SO
Exp.	6.135 [18]	55.1 [57] 58.2 [58]		1.615 [60] 1.696 [18]	670 [62] 673 [50] 750 [63]
Other works	6.167 [45] 6.118 [45] 6.23 [55] 6.08 [56] 6.09 [47]	54.412 [45] 56.440 [45] 49 [55] 56 [56] 56.1 [47]	4.109 [45] 4.253 [45] 4.28 [55] 4.31 [56] 4.362 [47]	1.47 [46] 1.29 [40]	630 [40] 658 [51] 640 [64]

For $GaP_{1-x}Sb_x$ alloys, Stringfellow group observed from an absorption spectra measurements [69] that single-line peaks at 1.14eV for $GaP_{0.53}Sb_{0.47}$ and at 1.625eV for $GaP_{0.76}Sb_{0.24}$ are in good agreement with the SOI-mBJ calculated values of 1.146 eV for $GaP_{0.5}Sb_{0.5}$ and 1.787eV for $GaP_{0.75}Sb_{0.25}$ and these values are more accurate than the recent ones calculated using projector augmented wave method with negligible SOI [14]. For $GaP_{0.25}Sb_{0.75}$ ternary alloy, our calculated band-gap width is 0.631(0.68)eV, which agrees well with the corresponding Chen and Ravindra results presented within parenthesis [14].

For $AlP_{1-x}Sb_x$ alloys and from our calculations for the band-gap energies, we expect that the obtained results will be tested, to confirm their reliability, in future both theoretically and as well as experimentally.

In figure 5, we display the composition dependence of the calculated band gaps of the two ternary alloys using mBJ scheme. The band gap increases nonlinearly with increasing concentration x providing a positive band-gap bowing (it is a parameter describing the deviation from linearity). Indeed, it is a general trend to describe the band gap of an alloy $AB_{1-x}C_x$ in terms of the energy gaps of the pure compound E_{AB} and E_{AC} by the semi-empirical formula:

$$E_g = (1-x)E_{AB} + xE_{AC} - x(1-x)b, \quad (1)$$

where the curvature b is commonly known as the gap bowing parameter. The values of b obtained by quadratic fit are 1.412 and 1.552 eV for $AlP_{1-x}Sb_x$ and $GaP_{1-x}Sb_x$ respectively obtained using SOI-mBJ calculation. In order to understand the physical origins of band-gap bowing, it can be routinely decomposed into three contributions resulting from volume deformation, charge transfer and bond length relaxation [70,71].

On the other hand, the energy of spin-orbit interaction Δ_{SO} is calculated for both $AlP_{1-x}Sb_x$ and $GaP_{1-x}Sb_x$ ternary alloys and their binary compounds. The SOI of

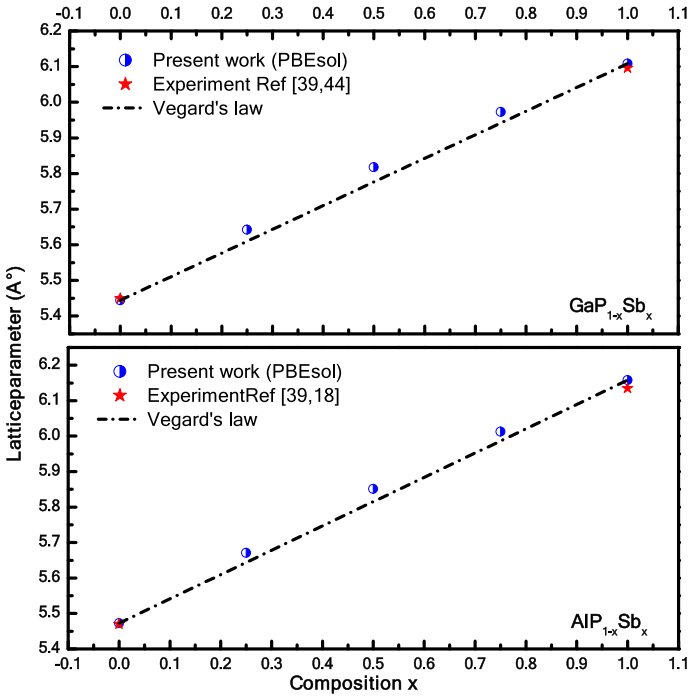

Figure 1. Composition dependence of the calculated lattice constant of $GaP_{1-x}Sb_x$ and $AlP_{1-x}Sb_x$ alloys using GGA-PBEsol.

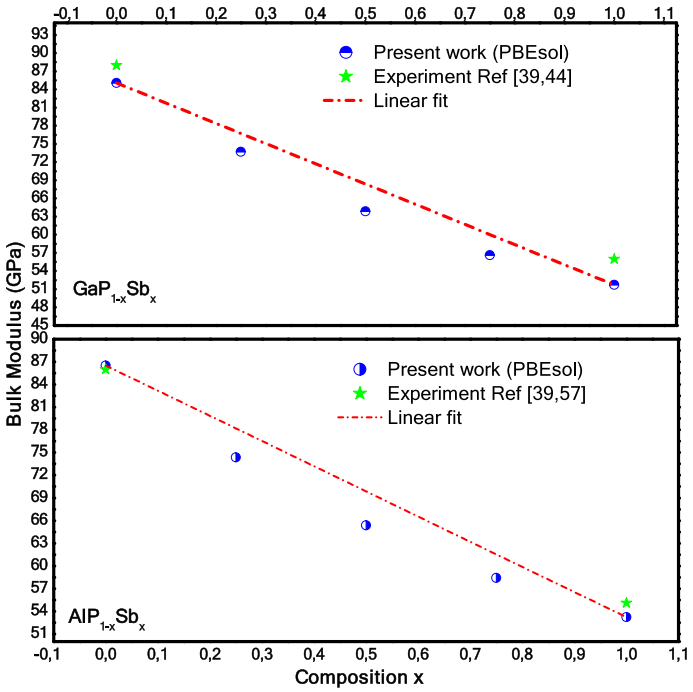

Figure 2. Composition dependence of the calculated bulk modulus of $GaP_{1-x}Sb_x$ and $AlP_{1-x}Sb_x$ alloys using GGA-PBEsol.

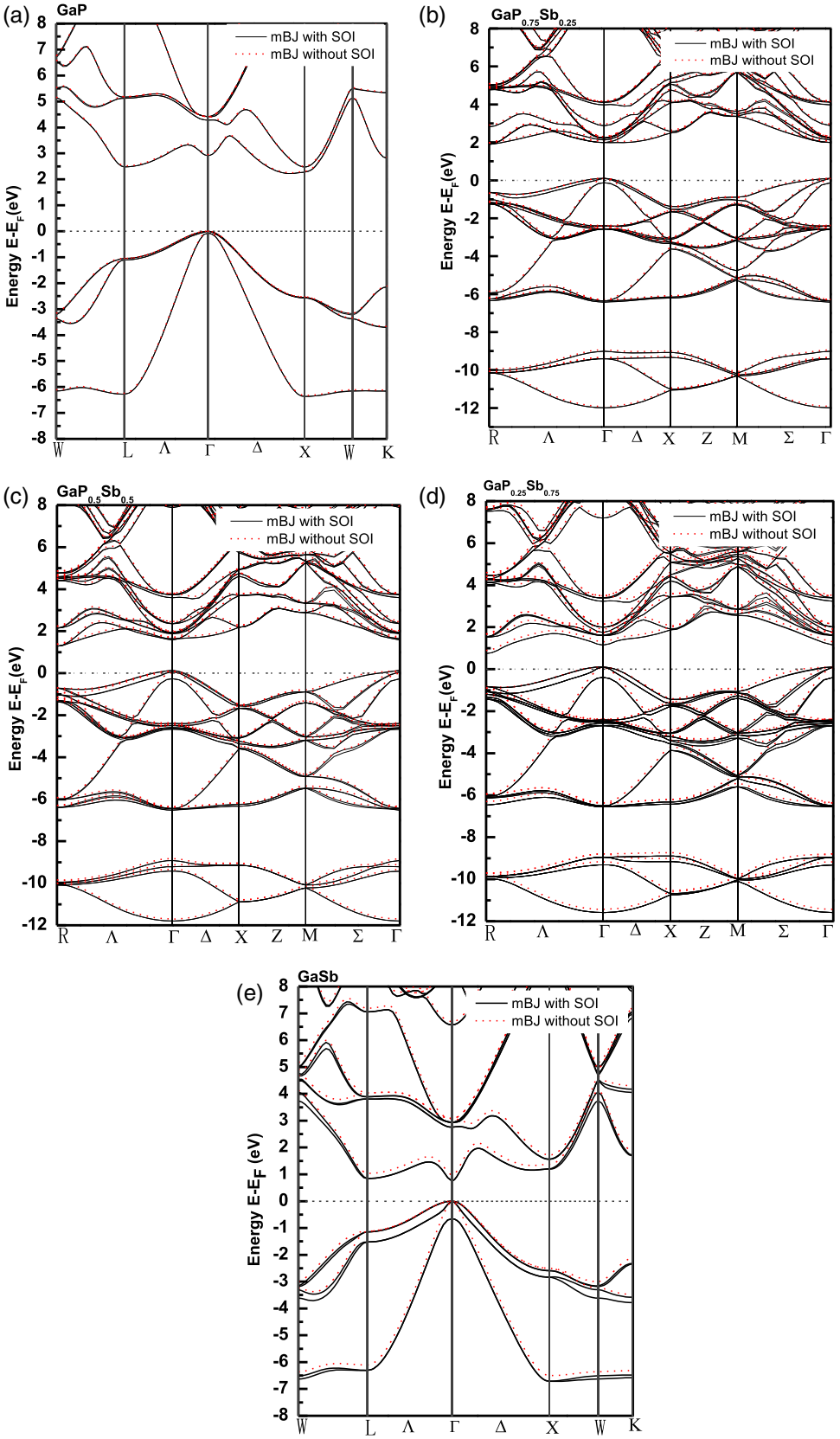

Figure 3. Band structures along the high-symmetry lines of GaP, $GaP_{0.75}Sb_{0.25}$, $GaP_{0.5}Sb_{0.5}$, $GaP_{0.25}Sb_{0.75}$ and GaSb. mBJ approximations without SOI and with SOI are shown in dotted and solid lines, respectively.

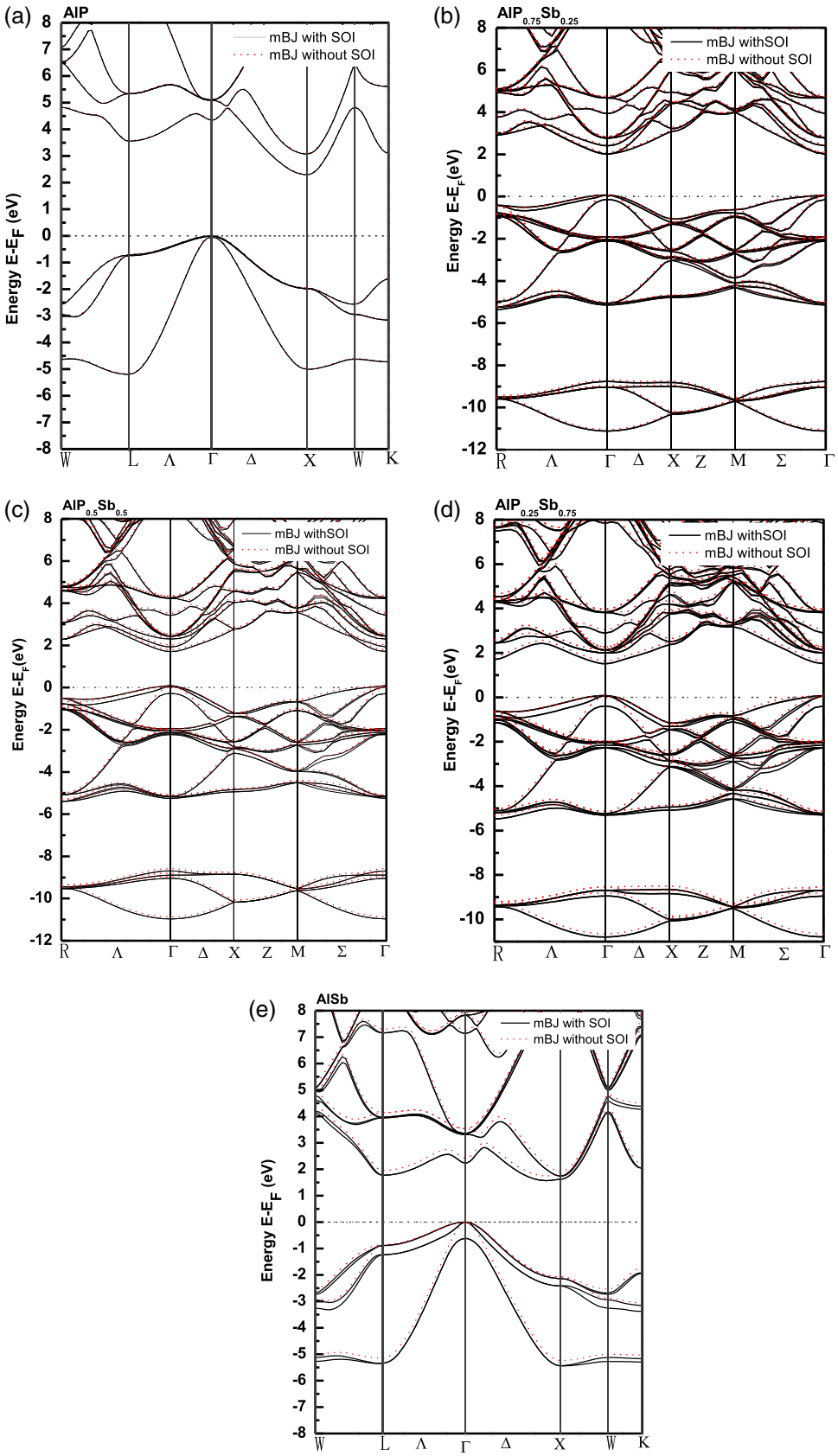

Figure 4. Band structures along the high-symmetry lines of AlP, $AlP_{0.75}Sb_{0.25}$, $AlP_{0.5}Sb_{0.5}$, $AlP_{0.25}Sb_{0.75}$ and AlSb. mBJ apprroximations without SOI and with SOI are shown in dotted and solid lines, respectively.

semiconductors at Γ-point leads basically to a splitting of the highest valence p-bands into $p_{1/2}$ band (Γ_{7v}) and $p_{3/2}$ band (Γ_{8v}). This SO splitting is defined as

$$\Delta_{SO} = E(\Gamma_{8v}) - E(\Gamma_{7v}).$$

Our calculated values of spin-orbit (SO) splitting are given in tables 1 and 2 where good agreement is found with available theoretical calculations and experimental data. We found that the SO splitting becomes strong for AlSb and GaSb and corresponds to 620.39 and 655.69 meV respectively, compared with the weak SO splitting of the light compounds such as AlP (53.73 meV) and GaP (72.69 meV). The remarkable importance of the SO splitting of AlSb and GaSb compounds is a consequence of the stabilisation(destabilisation) of the $p_{1/2}$ ($p_{3/2}$) orbital energies.

It is clear that the SO coupling is important in antimony-based semiconductors. Thus, it has been taken into consideration to study the electronic properties of the two considered ternary alloys. Figure 5 shows the variation of this property with Sb concentration. Generally, Δ_{SO} increases with Sb concentration. The significant increase of Δ_{SO} with increasing Sb composition is attributed to the large atomic mass of Sb which increases the interaction between the electron spin and orbital angular momentum.

A reasonable fitting of our calculated data corresponding to the $AlP_{1-x}Sb_x$ and $GaP_{1-x}Sb_x$ alloys varies almost linearly with a marginal upward bowing parameter equal to 0.085 and 0.086 eV respectively which is in agreement with most of the studies [18], which showed that the split-off gap of most of the III–V ternary semiconductor alloys can be fitted quite well by linear interpolation.

We can note that our calculations of the band gap of $AlP_{1-x}Sb_x$ and $GaP_{1-x}Sb_x$ alloys show strong non-linear dependence region which expand from the visible range of wavelengths to the infrared range making the material under study extremely interesting. This is why they have been selected and recommended for use in a variety of new devices.

For more explanation of the nature of the electronic band structure, we present and analyse the computed total and partial densities of states (TDOS/PDOS) for $AlP_{1-x}Sb_x$ and $GaP_{1-x}Sb_x$ alloys ($0 \leq x \leq 1$) using mBJ scheme with SOI, i.e. the prediction of the contribution of each atomic character to these bands by dividing the total DOS into s, p and d orbitals. It is observed that the TDOS of all the binary compounds (the plots are not displayed) are divided into two fundamental regions, the valence band (VB) and conduction band (CB). The upper region of the VB is formed by the hybridisation between both Al_s and Sb_p states for AlSb, Al_s and P_p for AlP, Ga_s and Sb_p for GaSb and Al_s and Sb_p for AlSb, while the bottom of the CB is mainly occupied by the Al_s/p states for AlP and AlSb, by Ga_s/p states for both GaP and GaSb.

Referring to figures 6 and 7, TDOS and PDOS of the two considered ternary alloys at different x concentrations have great similarity and unique behaviour except the magnitude of the peaks that varies with respect to the values of x and the type of the studied compounds. It is remarkable that for all the considered materials, the TDOS is divided into three main regions, two located in the VB, the lower valence band (VB_{low}), higher valence band (VB_{higher}) and the conduction band. VB_{low} is mainly dominated by the P_s and Sb_s states for both $GaP_{1-x}Sb_x$ and $AlP_{1-x}Sb_x$ ternary alloys. VB_{higher} is divided into two sub-bands. The first one is mainly occupied by Ga_s and P/Sb_p states in the case of $GaP_{1-x}Sb_x$ and by Al_s and P/Sb_p states in the case of $AlP_{1-x}Sb_x$, while the second one is mainly dominated by Ga/P/Sb_p states for $GaP_{1-x}Sb_x$ and by Al/P/Sb_p states for $AlP_{1-x}Sb_x$ ternary alloys. On the other hand, the contribution in the bottom of the CB is principally composed of a mixture of Ga_s and P/Sb_p states for $GaP_{1-x}Sb_x$ and of Al_s and P/Sb_p states for $GaP_{1-x}Sb_x$ while the remaining part is mainly formed with Ga/P/Sb_p states for $GaP_{1-x}Sb_x$ and with Al/P/Sb_p states for $AlP_{1-x}Sb_x$.

3.3 *Thermodynamic properties*

In this section, we present a rigorous theoretical study of the thermodynamic properties of $GaP_{1-x}Sb_x$ and $AlP_{1-x}Sb_x$ alloys based on the regular-solution model [72]. The calculations carried out here are based on *ab-initio* method. We calculate the Gibbs free energy of mixing $\Delta G_m(x, T)$ which allows us to access the T–x phase diagram and obtain the critical temperature, T_c, for miscibility. Details of the calculations are given in refs [73,74]. Indeed, an important contribution arises from the mixing enthalpy, which can be obtained from the calculated total energies as

$$\Delta H_m = E_{AB_{1-x}C_x} - (1-x)E_{AB} - xE_{AC}, \qquad (2)$$

where $E_{AB_{1-x}C_x}$, E_{AB} and E_{AC} are the energies of $AB_{1-x}C_x$ alloy, and the binary compounds AB and AC respectively. We then calculated ΔH_m to obtain Ω as a function of concentration. The calculated values of the formation enthalpies for alloys of interest are summarised in table 3. Comparison with the available data has been made wherever possible. The values obtained are in good agreement with the previous theoretical calculations of Chen and Ravindra [14]. From our results we can remark that for a given composition, the calculated values show that the mixing enthalpy decreases

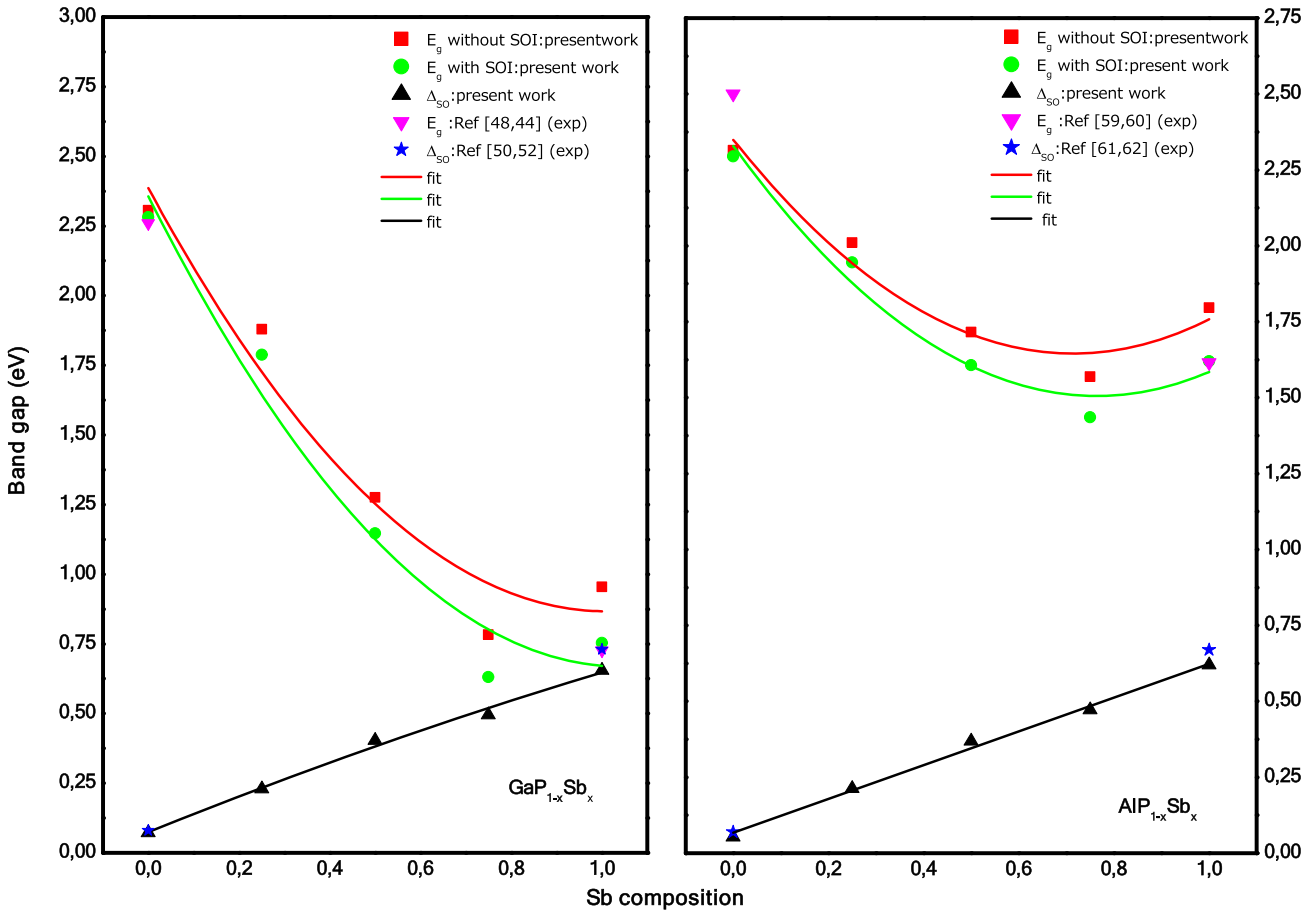

Figure 5. Energy band gap and spin-orbit splitting energy in $GaP_{1-x}Sb_x$ and $AlP_{1-x}Sb_x$ alloys as a function of Sb concentration.

from AlPSb to GaPSb. This is due to the smaller lattice mismatch and smaller bulk modulus in GaPSb. This smaller lattice mismatch leads to smaller strain energy and thus smaller formation enthalpy.

The results show that the mixing enthalpy does not monotonically decrease from GaP to GaSb. Instead, ΔH_m is smaller in $GaP_{0.75}Sb_{0.25}$ and $GaP_{0.25}Sb_{0.75}$ and larger in $GaP_{0.5}Sb_{0.5}$. The same trend is also found in Al compounds. This is because the large degree of alloy mixture induces more strain energy and hence larger formation enthalpy. This also explains the hold of large range miscibility gap in the phase diagram shown later. We note that the values of the enthalpy of mixing are all positive, which is the trend of all III–V semiconductors alloys [75].

By using the expression $\Omega = \Delta H_m/x(1-x)$, we can calculate, for each x, the value of Ω from the above DFT values of ΔH_m. The interaction parameter Ω depending on x is then obtained from a linear fit to the Ω values. The best fit gives

$$GaP_{1-x}Sb_x \Longrightarrow \Omega(\text{kcal/mol}) = 15.607 - 13.376x \tag{3}$$

$$AlP_{1-x}Sb_x \Longrightarrow \Omega(\text{kcal/mol}) = 15.959 - 3.350x. \tag{4}$$

The average value of x-dependent Ω in the range $0 \leq x \leq 1$ derived from those equations for $GaP_{1-x}Sb_x$ alloy is 8.919 kcal/mole and for $AlP_{1-x}Sb_x$ is 14.284 kcal/mole.

The larger enthalpy for $GaP_{1-x}Sb_x$ and $AlP_{1-x}Sb_x$ alloys suggests a large value of Ω and, hence a higher critical temperature. By calculating free energy of mixing,

$$\Delta G_m = \Delta H_m - RT[x \ln x + (1-x)\ln(1-x)], \tag{5}$$

where R is the gas constant and T is the absolute temperature. We determine the temperature–composition phase diagram, in which the critical temperature, the stable, metastable and unstable composition can be obtained. In the region above T_c, the solid solution is miscible in all proportions. Below T_c the two binodal points are determined as those points at which the common tangent line touches the ΔG_m curves. The two spinodal points are determined as those points at which the second derivative of ΔG_m is zero; $\delta^2(\Delta G_m)/\delta x^2 = 0$.

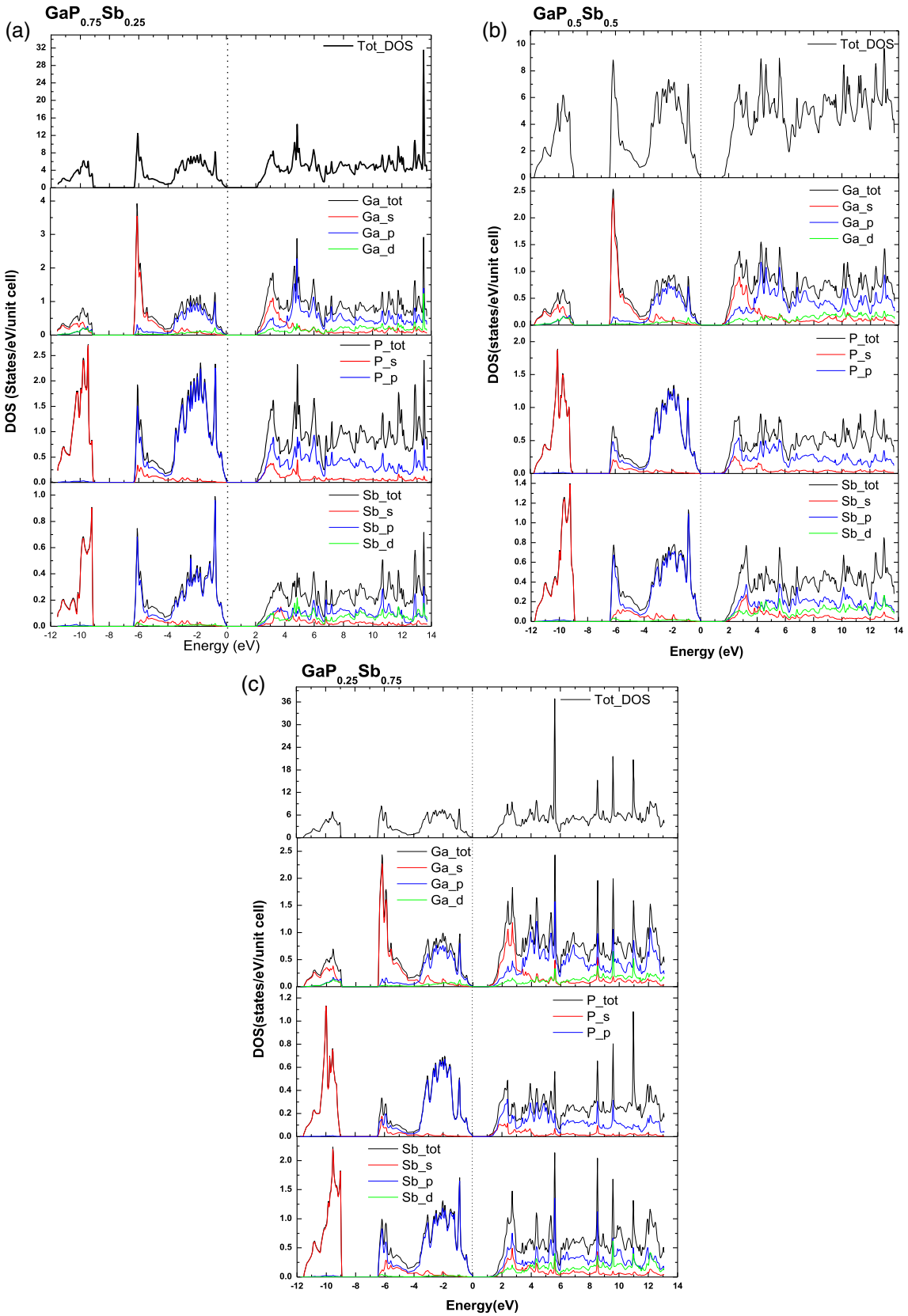

Figure 6. Total and partial density of states of $GaP_{1-x}Sb_x$ alloys for $x = 0.25$, 0.5 and 0.75 using mBJ functional with SOI. Fermi level is indicated by dashed line.

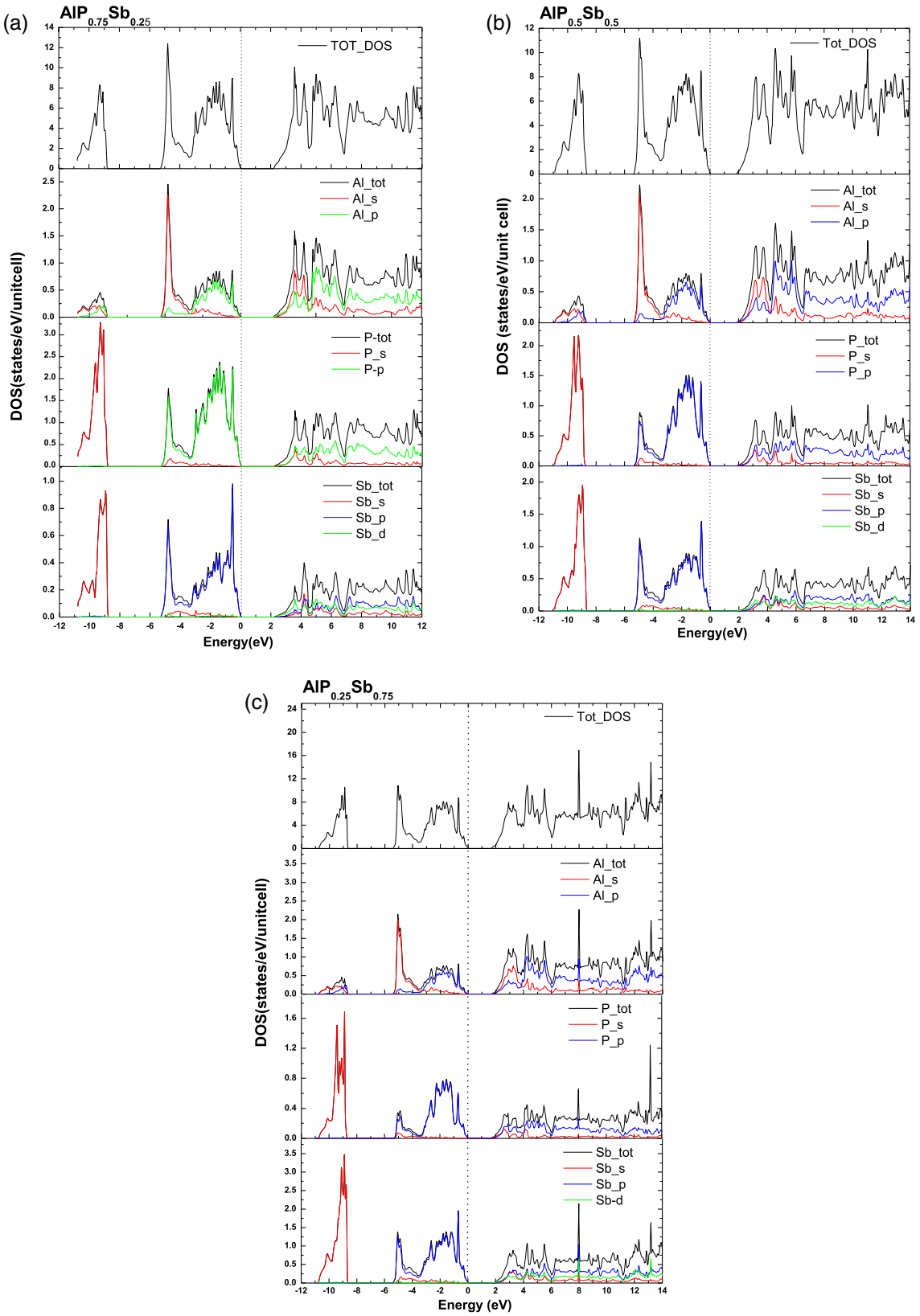

Figure 7. Total and partial density of states of $AlP_{1-x}Sb_x$ alloys for $x = 0.25$, 0.5 and 0.75 using mBJ functional with SOI. Fermi level is indicated by dashed line.

Table 3. The calculated value of enthalpy of mixing ΔH_m of $GaP_{1-x}Sb_x$ and $AlP_{1-x}Sb_x$ alloys for different compositions x.

	Enthalpy of mixing (eV/atom)	
Alloy	Our calculations	Literature [14]
$GaP_{0.75}Sb_{0.25}$	0.095	0.060
$GaP_{0.5}Sb_{0.5}$	0.109	0.071
$GaP_{0.25}Sb_{0.75}$	0.041	0.048
$AlP_{0.75}Sb_{0.25}$	0.122	–
$AlP_{0.5}Sb_{0.5}$	0.156	–
$AlP_{0.25}Sb_{0.75}$	0.109	–

The binodal curve or coexistence curve in the phase diagram describes the limits of solid solubility, i.e. the miscibility gap. Figure 8 shows the calculated phase diagram including the spinodal and binodal curves for the alloys of interest. We have calculated the phase diagram by using the average value of the x-dependent Ω, and hence the phase diagram looks symmetric. For temperatures and compositions above the spinodal curve, a homogeneous alloy is predicted. The wide range between this curve and binodal curves indicates that the alloy may exist as a metastable phase in which the order and disorder phases simultaneously exist. The critical alloy formation temperature occurs at a point where both the first and second derivatives of the free energy are zero, i.e. the plot has no curvature. The miscibility gap disappears at T_c. We observed a critical temperature $T_c = 2246$ K and a miscibility gap ranging from $x = 0.004$ to 0.99 at 530°C (803 K), covering essentially the entire ranging of solid composition for $GaP_{1-x}Sb_x$, close to the predicted results of Stringfellow [75] with a calculated critical temperature of 1996 K and a miscibility gap ranging from $x = 0.01$ to 0.99 at the same temperature. For $AlP_{1-x}Sb_x$ alloys, we observed a critical temperature $T_c = 3596$ K. Concerning this alloy, no theoretical works or experimental data were published in the literature.

For the considered phase diagram, more stable semiconductor alloys are likely to form at high temperature and these results indicate that the alloys are unstable over a wide range of intermediate compositions at normal growth temperature.

Finally, to investigate some thermal properties, we used the quasiharmonic Debye model as implemented in the Gibbs program [76]. Through the quasiharmonic Debye model, one could calculate the thermodynamic quantities of any temperatures and pressures of compounds from the calculated E–V data. The theoretical details of this procedure are available in ref. [76]. The thermal properties are determined in the temperature

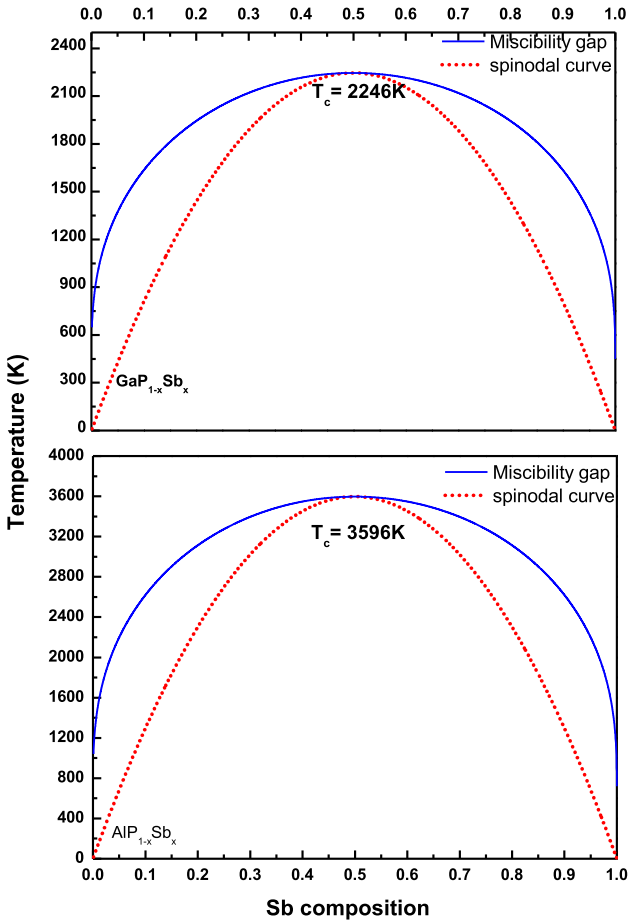

Figure 8. Phase diagram of $GaP_{1-x}Sb_x$ and $AlP_{1-x}Sb_x$ alloys as a function of Sb concentration. Solid line represents miscibility gap and dotted line represents spinodal curve.

range 0–600 K, where the quasiharmonic model remains fully valid. The pressure effect is studied within 0–10 GPa.

Debye temperature is a fundamental thermodynamical parameter that is directly related to many physical properties of solids, such as elastic constants, melting temperature, specific heat and it is an important characteristic of the temperature of solids. When the temperature rises above absolute zero, the atoms of the solid gradually vibrate to Debye's temperature. This represents the temperature at which the vibrations reach their maximum possible modes. It is a good approximation of the hardness of solids. Figure 9 shows the Debye temperature θ_D as a function of temperature for $GaP_{0.25}Sb_{0.75}$ and $AlP_{0.75}Sb_{0.25}$ ternary alloys at different pressures. At a given pressure, θ_D is found to be nearly constant from 0 to 100 K. In this temperature range, the anharmonicity is low and the crystal expands very little with increasing temperature. At low temperatures, one expects

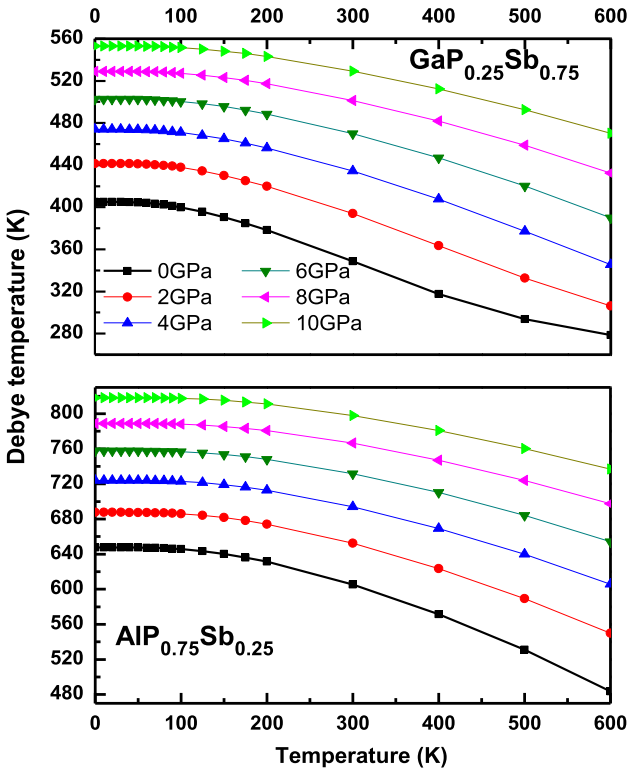

Figure 9. Debye temperature θ_D vs. temperature at some fitted pressures for the $GaP_{0.25}Sb_{0.75}$ and $AlP_{0.75}Sb_{0.25}$ alloys.

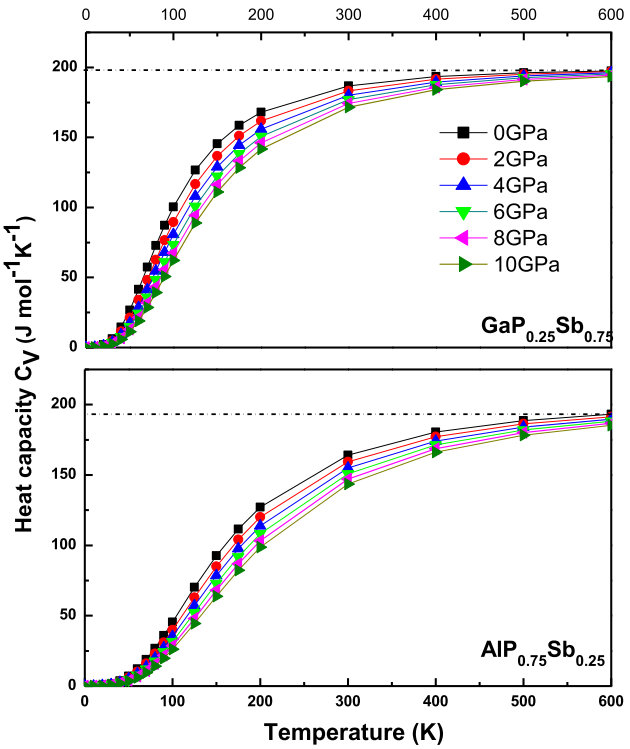

Figure 10. Temperature dependence of the constant volume heat capacity C_V at some fitted pressures for the $GaP_{0.25}Sb_{0.75}$ and $AlP_{0.75}Sb_{0.25}$ alloys.

the high-frequency modes to be frozen, i.e., vibrational excitations arise only from acoustic vibrations. θ_D diminishes quite linearly with increasing temperature, indicating the change in the vibrational spectrum of the atoms with temperature. θ_D is associated with the maximum crystal vibration frequency for a given structure and symmetry. At room temperature and zero pressure, the values of Debye temperature are 348.60 and 605.48 K for $GaP_{0.25}Sb_{0.75}$ and $AlP_{0.75}Sb_{0.25}$, respectively. The variations of heat capacity C_V with temperature at different pressures for $GaP_{0.25}Sb_{0.75}$ and $AlP_{0.75}Sb_{0.25}$ ternary alloys are presented in figure 10. From this figure, for low temperature, the proportionality of heat capacity to T^3 is clear as given in Debye model. C_V increases rapidly with temperature due to the enhanced anharmonic effect at elevated temperatures, while for higher temperatures it tends to the classical Dulong–Petit limit, approximately to 197.414 and 193.214 (J mol^{-1} K^{-1}) for $GaP_{0.25}Sb_{0.75}$ and $AlP_{0.75}Sb_{0.25}$, respectively, indicating that all the phonon modes are excited. In addition, C_V increases with the increase in temperature at a given pressure and slightly decreases with the pressure rise at a given temperature. The effects of temperature on the heat capacity at low temperatures (below θ_D) are very significant.

4. Conclusions

In this study, we have presented a complete theoretical analysis of the structural, electronic and thermodynamic properties of $GaP_{1-x}Sb_x$ and $AlP_{1-x}Sb_x$ alloys for a number of ordered structures and compositions using the FP-LAPW+lo method within DFT. The composition dependence of the lattice constant and bulk modulus is investigated. The lattice constants of $GaP_{1-x}Sb_x$ and $AlP_{1-x}Sb_x$ exhibit a large deviation from Vegard's law which is mainly due the large mismatch between the lattice constants of the parent binary compounds. A significant deviation of the bulk modulus from linear concentration dependence is observed for these alloys. Our results of the lattice constant for $GaP_{1-x}Sb_x$ alloys are in excellent agreement with the available results reported in literature. The inclusion of SOI has significant contribution in explaining the band structure of $GaP_{1-x}Sb_x$ and $AlP_{1-x}Sb_x$ within the mBJ scheme. The inclusion of the SOI decreases the band gap by shifting the CB towards lower energies and gives the value of the band-gap energies for $GaP_{1-x}Sb_x$ alloys to be in close agreement with experimental results of Stringfellow group. With the inclusion of SOI, the band structures show topological semiconductor character with a positive energy gap for all ranges of concentrations for the

two considered ternary alloys. Therefore, the magnitude of the SO splitting Δ_{SO} grows with Sb concentration and fits quite well by linear interpolation. Finally, it is expected that these alloys are attractive materials which find applications in optoelectronic devices and solar cell applications in the infra-red (IR) and visible regions.

The calculated phase diagrams reveal that $GaP_{1-x}Sb_x$ and $AlP_{1-x}Sb_x$ alloys exhibit a significant phase miscibility gap and indicate that these alloys are stable at high temperature. Debye model is successfully applied to determine θ_D and heat capacity C_V for temperatures up to 600 K for a given pressure.

The reported calculations for $AlP_{1-x}Sb_x$ ternary alloys are newly investigated. Hence, this contribution is to cover the lack of data in the literature for these ternary alloys and add to the limited theoretical effort explored in the fundamental properties of $GaP_{1-x}Sb_x$ ternary alloys.

References

[1] R M Biefeld and S R Kurtz, Infrared detectors and emitters, in: Materials and devices, *Electronic Materials Series 8* edited by P Capper, C T Elliot (Kluwer Academic Publishers, Boston, 2000) p. 205

[2] R M Biefeld, A A Alleman, S R Kurtz and K C Baucom, *J. Crystal Growth* **195**, 356 (1998)

[3] S R Kurtz, A A Alleman, R M Biefeld and K C Baucom, *Appl. Phys. Lett.* **72**, 2093 (1998)

[4] R M Biefeld, A A Alleman and S R Kurtz, *Mater. Sci. Eng. B* **51**, 1 (1998)

[5] J R Soderstrom, J Y Yao and T G Andersson, *Appl. Phys. Lett.* **58**, 708 (1991)

[6] T Ashley, A B Dean, C T Eliott, C F McConville, G J Pryce and C R Whitehouse, *Appl. Phys. Lett.* **59**, 1761 (1991)

[7] R M Biefeld, *Mater. Sci. Eng. R* **36**, 105 (2002)

[8] H Shimomura, T Anan and S Sugou, *J. Crystal Growth* **162**, 121 (1996)

[9] S Saib and N Bouarissa, *Solid-State Electron.* **50**, 763 (2006)

[10] D Chen and N M Ravindra, *J. Mater. Sci.* **47**, 5735 (2012)

[11] O Hildebrandt, W Kuebart and M H Pilkuhn, *Appl. Phys. Lett.* **37**, 801 (1980)

[12] E H Reihlen, M J Jou, Z M Fang and G B Stringfellow, *J. Appl. Phys.* **68**, 4604 (1990)

[13] M J Jou, Y T Cherng, H R Jen and G B Stringfellow, *Appl. Phys. Lett.* **52**, 549 (1988)

[14] D Chen and N M Ravindra, *Emerging. Mater. Res.* **2**, 109 (2013)

[15] A R Degheidy and E B Elkenany, *Thin Solid Films* **599**, 113 (2016)

[16] A R Degheidy and E B Elkenany, *Mater. Chem. Phys.* **157**, 108 (2015)

[17] F Oumelaz, O Nemiri, A Boumaza, S Ghemid, H Meradji, S Ben Omran, F El Haj Hassan, D P Rai and R Khenata, *Indian J. Phys.* **92**, 705 (2018)

[18] I Vurgaftman, J R Meyer and L R Ram-Mohan, *J. Appl. Phys.* **89**, 5815 (2001)

[19] A Alahamry, N Bouarissa and A Kamli, *Physica B* **403**, 1990 (2008)

[20] N E H Fares and N Bouarissa, *Mater. Res.* **21(4)**, e20170964 (2018)

[21] A R Degheidy, E B Elkenany and O A Alfrnwani, *Comput. Condensed Matter.* **16**, e00310 (2018)

[22] H Shimomura, T Anan, K Mori and S Sugou, *Electron. Lett.* **30**, 314 (1994)

[23] T Anan, H Shimomura and S Sugou, *Electron. Lett.* **30**, 2138 (1994)

[24] J Wu and Z M Wang, *Quantum dot solar cells* (Springer, New York, Heidelberg, Dordrecht, London, 2014)

[25] E Lendvay, *Prog. Crystal Growth Charact.* **8**, 371 (1984)

[26] E C Muller and J C Richards, *J. Appl. Phys.* **35**, 1233 (1964)

[27] P Hohenberg and W Kohn, *Phys. Rev.* **136**, 864 (1964); W Kohn and L J Sham, *Phys. Rev. A* **140**, 1133 (1965)

[28] G K H Madsen, P Blaha, K Schwarz, E Sjöstedt and L Nordström, *Phys. Rev. B* **64**, 195134 (2001)

[29] K Schwarz, P Blaha and G K H Madsen, *Comput. Phys. Commun.* **147**, 71 (2002)

[30] P Blaha, K Schwarz, G K H Madsen, D Kvasnicka and J Luitz, *WIEN2k, An Augmented-Plane-Wave + Local Orbitals Program for calculating crystal properties* (Karlheinz Schwarz, Techn. Universitat, Wien, Austria, 2001)

[31] J P Perdew, A Ruzsinszky, G I Csonka, O A Vydrov, G E Scuseria, L Constantin, X Zhou and K Burke, *Phys. Rev. Lett.* **100**, 136406 (2008)

[32] J P Perdew, K Burke and M Ernzerhof, *Phys. Rev. Lett.* **77**, 3865 (1996)

[33] F Tran and P Blaha, *Phys. Rev. Lett.* **102**, 226401 (2009)

[34] H J Monkhorst and J D Park, *Phys. Rev. B* **13**, 5188 (1976)

[35] F D Murnaghan, *Proc. Nat. Acad. Sci. USA* **30**, 5390 (1944)

[36] B Fluegel, S Francoeur and A Mascarenhas, *Phys. Rev. Lett.* **97**, 067205 (2006)

[37] D J Chadi, *Phys. Rev. B* **16**, 790 (1977)

[38] Y Zhang, A Mascarenhas and L W Wang, *Phys. Rev. B* **71**, 155201 (2005)

[39] K H Hellwege and O Madelung (Eds.), Semi-conductor, intrinsic properties of group IV elements and III–V, II–VI and I–VII compounds, in: *Landolt-Bornstein new series, Group III* (Springer, Berlin, 1982) Vol. 22

[40] M Briki, M Abdelouhab, A Zaoui and M Ferhat, *Superlatt. Microstruct.* **45**, 80 (2009)

[41] R Ahmed, F Aleem, S J Hashemifar and H Akbarzadeh, *Physica B* **403**, 1876 (2008)

[42] O Madelung and Landolt Bornstein, *Numerical data and functional relationships in science and technology new series* (Springer, Berlin, 1982)

[43] B Bouhafs, H Aourag and M Cartier, *J. Phys. Condens. Matter* **12**, 5655 (2000)
[44] S Adachi, *J. Appl. Phys.* **58**, R1 (1985)
[45] H Salehi, H A Badehian and M Farbod, *Mater. Sci. Semicond. Process*. **26**, 477 (2014)
[46] F El Haj Hassan, A Breidi, S Ghemid, B Amrani, H Meradji and O Pagès, *J. Alloys Compd*. **499**, 80 (2010)
[47] S Q Wang and H Q Ye, *Phys. Rev. B* **66**, 235111 (2002)
[48] M Levinshtein, S Rumyantsev and M Shur (Eds.), *Handbook series on semiconductor parameters* (World Scientific, 1996)
[49] M P Thompson, G W Auner, T S Zheleva, K A Jones, S J Simko and J N Hilfiker, *J. Appl. Phys*. **89**, 3321 (2001)
[50] A N Chantis, M V Schilfgaarde and T Kotani, *Phys. Rev. Lett*. **96**, 086405 (2006)
[51] P Carrier and S H Wei, *Condens. Matter* **2**, 0403409 (2004)
[52] B J Parsons and H Piller, *Program and abstract of the 3rd materials science symposium, electronic density of states* (Gaitherburg, MD, USA, 1969)
[53] *Semiconductors: Basic data*, 2nd edn, edited by O Madelung (Springer, Berlin, 1996)
[54] F Annane, H Meradji, S Ghemid and F El Haj Hassan, *Comput. Mater. Sci*. **50**, 274 (2010)
[55] A Rashid, E A Fazal, S J Hashemifar, R Haris and H Akbarzadeh, *Commun. Theor. Phys.* **52**, 527 (2009)
[56] Z N Liang, P J H Denteneer and L Niesen, *Phys. Rev. B* **52**, 8864 (1995)
[57] K Strössner, S Ves, C K Kim and M Cardona, *Phys. Rev. B* **33**, 4044 (1986)
[58] R Weil, *J. Appl. Phys*. **43**, 4271 (1972)
[59] M Z Huang and W Y Ching, *Phys. Rev. B* **47**, 9449 (1993); M Z Huang and W Y Ching, *Phys. Rev. B* **47**, 9464 (1993)
[60] C Alibert, A Joullié, A M Joullié and C Ance, *Phys. Rev. B* **27**, 4946 (1983)
[61] S K Pugh, D J Dugale, S Brand and R A Abram, *Semicond. Sci. Technol*. **14**, 23 (1999)
[62] S Adachi, *Handbook on physical properties of semiconductors* (Kluwer Academic Publishers, New York, 2004)
[63] Landolt Börnstein, *Numerical data and functional relationships in science and technology* edited by O Madelung, M Schulz and H Weiss (Springer, Berlin, 1982) Vol. III/17a,b
[64] W P Huhn and V Blum, *Condens. Mater. Sci.* **2**, 1804 (2017)
[65] L Vegard, *Z. Phys.* **5**, 17 (1921)
[66] S Adachi, *Properties of semiconductor alloys: Group IV, III–V and II–VI semiconductors* (John Wiley & Sons, New York, 2009)
[67] A Fazeli Kisomi and S J Mousavi, *Pramana – J. Phys.* **91**: 18 (2018)
[68] D J Singh, *Phys. Rev. B* **82**, 205102 (2010)
[69] E H Reihlen, M J Jou, D H Jaw and G B Stringfellow, *J. Appl. Phys*. **68**, 760 (1990)
[70] A Zunger, S H Wei, L G Fereira and J E Bernard, *Phys. Rev. Lett*. **65**, 353 (1990)
[71] S H Wei, L G Fereira, J E Bernard and A Zunger, *Phys. Rev. B* **42**, 9622 (1990)
[72] R A Swalin, *Thermodynamics of solids* (Wiley, New York, 1961)
[73] L G Ferreira, S H Wei, J E Bernard and A Zunger, *Phys. Rev. B* **40**, 3197 (1989)
[74] L K Teles, J Furthmüller, L M R Scolfaro, J R Leite and F Bechstedt, *Phys. Rev. B* **62**, 2475 (2000)
[75] G B Stringfellow, *J. Crystal Growth* **98**, 108 (1989)
[76] M A Blanco, E Francisco and V Luaña, *Comput. Phys. Commun*. **158**, 57 (2004)